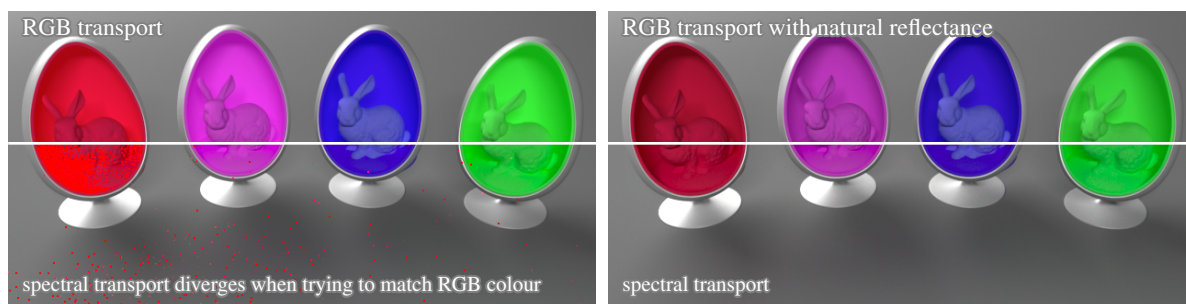


# Physically Meaningful Rendering using Tristimulus Colours

Johannes Meng<sup>†\*</sup> Florian Simon<sup>‡\*</sup> Johannes Hanika<sup>§</sup> Carsten Dachsbacher<sup>¶</sup>

Karlsruhe Institute of Technology

\*joint first authors.



**Figure 1:** Four chairs with diffuse reflectance defined in  $Rec. 709 \in [0, 1]^3$ . In results obtained using an RGB path tracer (top left), the indirect illumination seems to glow unnaturally, e.g. behind the bunnies. A spectral path tracer reveals why (bottom left): to reproduce the same colours, reflectance spectra must violate energy conservation, causing the render to diverge. With the mapping techniques we propose, colour values can be altered so that both the RGB and the spectral render produce physically plausible results (right images).

## Abstract

*In photorealistic image synthesis the radiative transfer equation is often not solved by simulating every wavelength of light, but instead by computing tristimulus transport, for instance using sRGB primaries as a basis. This choice is convenient, because input texture data is usually stored in RGB colour spaces. However, there are problems with this approach which are often overlooked or ignored. By comparing to spectral reference renderings, we show how rendering in tristimulus colour spaces introduces colour shifts in indirect light, violation of energy conservation, and unexpected behaviour in participating media.*

*Furthermore, we introduce a fast method to compute spectra from almost any given XYZ input colour. It creates spectra that match the input colour precisely. Additionally, like in natural reflectance spectra, their energy is smoothly distributed over wide wavelength bands. This method is both useful to upsample RGB input data when spectral transport is used and as an intermediate step for corrected tristimulus-based transport.*

*Finally, we show how energy conservation can be enforced in RGB by mapping colours to valid reflectances.*

Categories and Subject Descriptors (according to ACM CCS): Computer Graphics [I.3.7]: Three-Dimensional Graphics and Realism—Color, shading, shadowing, and texture;

## 1. Introduction

Physically-based rendering in computer graphics [PH10] solves the radiative transfer equation [Cha60]. To achieve

this for applications such as architectural design, product visualisation, and special effects in the movie industry, Monte Carlo ray tracing [Erm75, Sob94] is often used.

The input to such rendering systems may consist of 3D meshes for the shapes, material properties, and textures for the colours. Following Grassmann's law, these are usually stored in a tristimulus format, i.e. three values define a colour per texel [WS82]. The most well-known and most frequently used colour space for textures is sRGB [Rec02], which we

<sup>†</sup> meng@kit.edu

<sup>‡</sup> florian.simon@kit.edu

<sup>§</sup> hanatos@gmail.com

<sup>¶</sup> dachsbacher@kit.edu

refer to as `Rec. 709` for the linear (non-gamma corrected) version.

With high-quality wide-gamut output devices being widely available, but also for lossless storage and post-processing, there is a need for wide-gamut colour spaces. Currently, we can observe an ever growing abundance of different colour spaces, such as `AdobeRGB`, `ProPhotoRGB` and lately the *academy colour encoding specification (ACES)* colour space used in the movie industry. These tristimulus-based colour spaces provide a very large gamut; in fact, *ACES* covers the whole range of visible colours. However, this comes at the cost that some values  $\in [0, 1]^3$  represent physically impossible colours, i.e. *imaginary stimuli* which lie outside the spectral locus in the chromaticity diagram.

While it is obvious that such values cannot result in physically meaningful rendering when used as reflectances (e.g. to define a *bidirectional scattering distribution function*, BSDF), it is less obvious that even values inside the spectral locus do not always represent physical reflectances [Sch19]. This is due to the fact that a colour can either have very saturated chromaticity or be very bright.

We will use the term *solid of valid reflectances* to describe the set of all visible colours for which energy conserving spectra (i.e.  $\rho(\lambda) \leq 1$  for all wavelengths  $\lambda$ ) can be found. Unlike emission spectra, naturally occurring reflectance spectra are generally smooth [Mal86]. Therefore, we similarly introduce the *solid of natural reflectances*. It contains all colours for which a smooth and energy conserving, or *physically plausible*, reflectance spectrum can be found.

We also thoroughly analyse the differences between spectral and RGB transport (assuming same-speed transport, i.e. no fluorescence) with regard to ensuring physically plausible reflectances for both cases. Physically, light-matter interaction can be modelled as a component-wise multiplication of the incoming spectral radiance with a reflectance spectrum (i.e. the BSDF depends on the wavelength  $\lambda$ ). The results of tristimulus transport, however, heavily depend on the working colour space [Agl14]. Saturation, brightness and hue of indirect light depend on this “arbitrary” choice, since a component-wise spectrum multiplication is replaced by a component-wise tristimulus multiplication. Note that this cannot be corrected with a look-up table after rendering, since the colour shift will depend on the number of interactions of light before reaching the camera.

In summary, the contributions of our paper are:

- We show how tristimulus transport is not in general energy conserving in the physical sense, even though the methods converge mathematically (Sec. 2).
- We propose a fast method to compute smooth spectra from XYZ tristimulus input values which behave closely to natural spectra in light transport simulation (Sec. 3).
- We introduce a *mapping technique for physically plausible*

*reflectances*. This is essential for tristimulus workflows (such as traditional RGB texture painting or RGB output of shading languages) to ensure that produced texture data results in energy conserving BSDFs (Sec. 4).

- We analyse three strategies to perform this mapping: a) trivial but fast clamping of the corresponding spectrum, b) preserving the exact chromaticity of the input, and c) with minimal CIE  $\Delta E$  colour distortion (Sec. 4).
- We show how to design a correctly colour managed rendering pipeline based on RGB transport (Sec. 5).

## 2. Background and Previous Work

**Colour Spaces** Tristimulus colour spaces are based on the colour matching functions [Wri28, SG31]. Our implementation relies on the recommendations given in [CIE04]: we use the 1931 2° 5nm steps colour matching functions  $\bar{x}(\lambda), \bar{y}(\lambda), \bar{z}(\lambda)$  defined over the abridged interval  $\Lambda = [380, 780]$ nm, and integration by summation.

There is an abundance of colour spaces available today. We are interested in RGB-colour spaces (such as `sRGB` or `Rec. 709` [Rec02]), since these are commonly used to describe input colour to rendering systems (as opposed to CMYK-like spaces, which are commonly used for printing). A colour space is defined by the three *primaries*, which define what exactly red, green, and blue mean. This also fixes the location and shape of the gamut, as well as the *white point*, which is considered the neutral colour of the space. For the sake of describing reflectances, we consider only linear RGB colour spaces (i.e. scene-referred, no gamma correction or tone reproduction curves are applied) and use the equal-energy white point (CIE illuminant E, a constant spectrum over the visible wavelengths, to not bake any illumination tint into the surface properties).

To be able to compare these spaces, the XYZ colour space was introduced as a standard profile connection space [FBH98]. From there,  $(x, y)$  chromaticities are derived as  $x = X/(X + Y + Z)$  and  $y = Y/(X + Y + Z)$ . An interesting special case is when  $(X + Y + Z) = 1$  (unity brightness), since then  $X = x$  and  $Y = y$ , which will simplify our reasoning in Sec. 3. The XYZ white point is fixed at illuminant E ( $x = 1/3, y = 1/3$ ), which makes this space suitable for us to work with. For colour fundamentals, we refer to the textbook by Wyszecki and Stiles [WS82].

When converting between colour spaces, the different sizes of their domains in  $(x, y)$  space give rise to the problem of gamut mapping. There are very many different approaches in literature [Mor08]. Related to these, we describe techniques to map arbitrary XYZ colour input to the solid of valid reflectances.

Colour constancy methods [For90, FH00] try to avoid colour casts in output images due to coloured light sources, specifically light sources of different colour temperatures,

by ensuring the output lies within an a-priori known locus of valid reflectances. Similarly, Ward and Eydelberg-Vileshin [WEV02] propose rendering in a white-point adapted Sharp colour space to avoid perceived colour casts in the output image. In contrast, we strive not to avoid such colour casts, since we believe that they can be an important part of the artistic process. This especially applies to physically based rendering, where multiple different illuminants may be chosen, and their effect should be faithfully reproduced.

**Spectral Rendering** When simulating light transport per wavelength, colour management simplifies substantially. The rendering equation [Kaj86] is solved per wavelength, either by transporting full spectra (discretised into bins or with basis functions [Mey88, Pee93, SFCD99]), continuous wavelength sampling, or transporting several wavelengths at the same time, combining the results via multiple importance sampling [VG95, WND\*14]. The problem of upsampling RGB input textures to spectral data still needs to be solved in this case, including the issue that RGB input might not represent valid reflectances. We provide the theory and tools to perform both fast upsampling from RGB to spectral power distribution in almost the whole visible gamut, and mapping to the solid of valid reflectances (solid mapping).

**Spectral Energy Conservation** While upsampling RGB or XYZ input to spectral data representing radiance (or emission) is possible without considering energy conservation, it needs to be taken into account for surface reflection (BSDF). Energy conservation holds per wavelength, e.g. in the case of a diffuse BSDF we have for every  $\lambda$  individually:

$$1 \geq \int_{\Omega} \rho(\lambda) / \pi d\omega^\perp = \rho(\lambda) \int_{\Omega} 1 / \pi d\omega^\perp = \rho(\lambda). \quad (1)$$

This bounds the spectral reflectance distribution  $\rho(\lambda)$ . Similarly the coefficients of other BSDF models can be bound to ensure energy conservation.

**Spectral Upsampling** There are several approaches to convert XYZ values to spectral power distributions in literature.

MacAdam [Mac35a, Mac35b] implicitly defines an XYZ to spectrum conversion in his work on achieving the highest possible brightness for a given colour saturation in printing. The method is not limited to a specific input, but produces spectra which are only suitable for rendering to a limited extent. MacAdam's spectra consist of a single box function wrapping around the interval of definition  $\Lambda$  (i.e. only one rising and one falling edge). Fig. 2 shows a comparison of the shapes of the corresponding spectra, and Fig. 3 shows an unintuitive colour shift in the indirect illumination when using box spectra.

Glassner [Gla95, p.104] gives a family of conversions which take a set of three basis functions as input, for instance the monitor response curves or the first three Fourier bases.

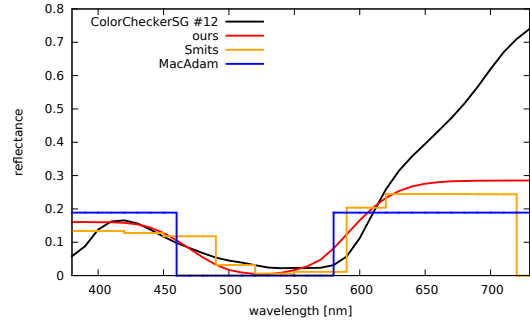


**Figure 2:** Comparison of four metameric spectra corresponding to the same XYZ values. Our method is the smoothest of the three upsampling strategies and also able to reproduce spectra for input outside the Rec. 709 gamut.

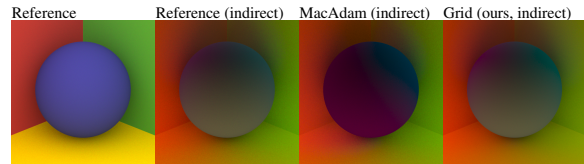


**Figure 3:** Spectral rendering of measured reflectances lit by illuminant F10 (a fluorescent light). The same tabulated data has been used in all images. MacAdam reflectance spectra cause strong colour shifts for indirect illumination. Our smooth spectra reproduce this much more faithfully. Images showing indirect illumination were scaled  $\times 4$  for display.

These methods can produce negative spectral power, which is a severe problem in physically based light transport simulation. Negative power will have to be clamped, resulting in uncontrolled colour shift.

The method by Smits [Smi99] is practical and widely adopted. It is based on a small set of ten precomputed box bases. They are optimised for smoothness and to match Rec. 709 primaries adapted to white point E, while obeying spectral energy conservation. Since these contradicting goals can only partly be met [Sch19], the resulting spectral output can be slightly larger than unity. Also, the method does not support round trips: converting a colour to spectrum and then back will result in a small, but noticeable colour cast. For instance the input XYZ = (1, 1, 1) results in a maximum spectrum value of 1.00012, and output XYZ = (.99945, .99942, .99982). This is not the worst case, and the difference seems small. However, with multiple interreflections and in the presence of bright light sources, colour shifts can be perceived. Furthermore, Smits' method is not designed to work with colours outside the Rec. 709 gamut. See Fig. 9 for an analysis of the perceptual error in- and outside this gamut. Finally, the optimisation performed to

obtain the set of box bases intrinsically depends on an RGB working space and does not work well for wide-gamut working spaces. This is discussed further in supplemental material. In our approach, we also use a nonlinear optimisation to find basis spectra, but change the interpolation scheme to be independent of the input colour space. Thus, our method can be seen as a generalisation of Smits' work.

Wang et. al. [WXS04] measure a set of reflectance spectra, and extend this set using Beer's Law. For upsampling, their technique linearly interpolates the basis spectra in three-dimensional XYZ space. The values for the measured spectra are not provided in [WXS04], and so reproducing the results is a challenge since measuring spectra requires special hardware. Also, it is not clear how well the solid of natural reflectances is covered by the extrapolation technique used in [WXS04]. Our method is conceptually similar, but instead of a three-dimensional search, we employ a very simple and efficient two-dimensional scheme.

All the works mentioned so far (including ours) ignore fluorescence at light interaction points, i.e. there is no crosstalk between wavelengths. Fluorescence has been considered in the print context [Cou07], but in the global illumination context, simulating light transport becomes significantly more involved. There have been some works to simulate fluorescence using Monte Carlo techniques [Gla94, WGRK\*97, WWLP06, SN07, BHD\*08, HHA\*10], but none of these implement full-featured bidirectional path tracing yet. We consider extending our work to fluorescence for future work.

### 3. Converting XYZ to Spectral Data

We are interested in upsampling arbitrary given XYZ input to a spectral power distribution, such that the result is physically meaningful in the sense that it resembles natural spectra as much as possible. In particular, we do not want to be limited by the Rec. 709 gamut. Also, the theoretical limit of MacAdam's spectra are too sharp for our purposes, since spectra derived this way produce unnaturally saturated indirect light with unexpected colour shifts (see Fig. 3). Lastly, the method should be efficient and suitable for evaluation at run-time.

First we consider finding a spectrum  $s(x, y, \lambda)$  for certain chromaticity coordinates  $(x, y)$  with unity brightness (i.e.  $b = X + Y + Z = 1$ ). For arbitrary brightness  $b$ , the spectrum  $s(X, Y, Z, \lambda)$  can be obtained by simple scaling, since the integral operator converting the spectrum to XYZ is linear. In a one-time precomputation we find the smoothest possible such spectra by performing a brute-force optimisation, described next, over sample points in the  $(x, y)$  chromaticity space.

#### 3.1. Optimisation

We search for discretised smooth spectra with 5nm steps in  $\Lambda$  which match the input  $(x, y)$  chromaticity. More

precisely, we minimise  $f(s) = \sum_{i=1}^{N-1} (s^{i+1} - s^i)^2$  subject to  $s^i \in [0, 1000] \forall i$  and  $\sum_i 5nm \cdot s^i \cdot (\bar{x}^i, \bar{y}^i, \bar{z}^i) = (x, y, 1 - x - y)$ , where  $s^i$  is the spectral value of bin  $i$  and  $(\bar{x}^i, \bar{y}^i, \bar{z}^i)$  are the tabulated colour matching functions. We use Python's `scipy` package to perform the optimisation (`scipy.optimize.minimize` with SLSQP, based on [Kra88]), and always start with an equal energy white spectrum.

The resulting spectra are smooth and mostly uni-modal, except for samples near the purple line, where two modes can be observed. There is some slight noise in the output due to the numerical minimisation, which also depends on the starting point, but overall we found the process to be stable (cf. Fig. 6, in which the maximum brightness was determined by per-pixel optimisation, and supplemental material, where we show our precomputed spectra). As opposed to MacAdam's optimal spectra [Mac35b], which consist of a simple box function, our spectra are more like natural spectra in terms of smoothness (see Fig. 2).

#### 3.2. Fast Implementation: Grid-based Upsampling

Since the optimisation process is slow, we precompute spectra for a set of points  $(x_i, y_i)$  offline (see Fig. 4) and store the resulting spectra  $s_i(\lambda) = s(x_i, y_i, \lambda)$ . Spectra  $s(x, y, \lambda)$  are then interpolated linearly from this precomputed set:

$$s(x, y, \lambda) = \sum a_i(x, y) s_i(\lambda). \quad (2)$$

To determine the weights  $a_i(x, y)$  quickly, we mostly use a regular grid topology with bilinear interpolation for inner points, and barycentric interpolation of triangle fans at the boundary of the spectral locus.

To better fit a grid to the spectral locus, we first rotate the  $(x, y)$  coordinate system into a new space  $x^*y^*$ , which first aligns the x axis with the purple line and then places the origin at the illuminant E white point  $(1/3, 1/3)$ .

The location of the grid points is then determined by regular sampling inside the spectral locus, where we make sure the most saturated red (lower right corner) lies exactly on a grid point. This makes sure the white point and the purple line can be sampled appropriately. The set is extended by a few points on the spectral line which form triangle fans together with the inner grid points. To smooth out interpolation artifacts, we also insert one more point at the center of gravity of all points generated in each boundary cell (see Fig. 4 for a grid with  $4 \times 6$  cells between white and red).

Finally, all grid locations are scaled towards the white point by a small adjustment factor  $1 - \epsilon$ . This step avoids numerical instabilities in the optimisation for colours near the spectral locus, but it also means that we cannot upsample some very saturated and monochromatic colours. This is further explained in supplemental material.

Simple calculus shows that each interpolated spectrum

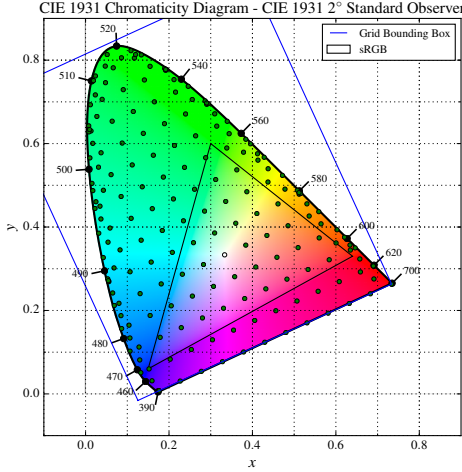


**Figure 4:** Visualisation of our grid of optimised spectra, overlaid on a chromaticity diagram, and the Rec.709 gamut. We use precomputed spectra at 186 sample points (green/white) to interpolate spectra at arbitrary  $(x, y)$  locations. There are  $4 \times 6$  grid cells between white and red.

$s(x, y, \lambda)$  will result in the correct chromaticity  $(x, y)$ :

$$\begin{aligned} X &= \int_{\Lambda} \bar{x}(\lambda) \cdot \sum a_i s_i(\lambda) d\lambda \\ &= \sum a_i \underbrace{\int_{\Lambda} \bar{x}(\lambda) \cdot s_i(\lambda) d\lambda}_{=X_i} \end{aligned} \quad (3)$$

if the weights  $a_i$  have been chosen such that  $x = \sum a_i x_i$  and  $y = \sum a_i y_i$ . From this we can see that if we interpolate the  $x, y$  chromaticities linearly, we will also interpolate the spectra linearly and vice versa. These spectra also satisfy  $X + Y + Z = 1$  if the input spectra  $s_i(\lambda)$  satisfy this condition:

$$\begin{aligned} X + Y + Z &= \sum a_i X_i + \sum a_i Y_i + \sum a_i Z_i \\ &= \sum_{i=1} a_i \underbrace{(X_i + Y_i + Z_i)}_{=1}. \end{aligned} \quad (4)$$

Note that we can always choose the brightness  $X_i + Y_i + Z_i = 1$  for all the sample spectra  $s_i(\lambda)$  by simple uniform scaling. Visually this means that we stay on the same 2D-slice through the spectral gamut, on the plane of  $(x, y)$  chromaticities which is used to visualise gamuts in 2D such as in Figs. 4 and 9.

Since the theoretically optimal spectra can be expressed by only one wrapped-around box function [Mac35b], smooth spectra close to this optimum will be similarly simple in shape. This can be observed when viewing our spectra in the supplemental material (Fig. 3–5). Hence there is no major difference between our interpolated spectra and the individually optimised ones, aside from very close to the purple line, where spectra are bi-modal and peaky.

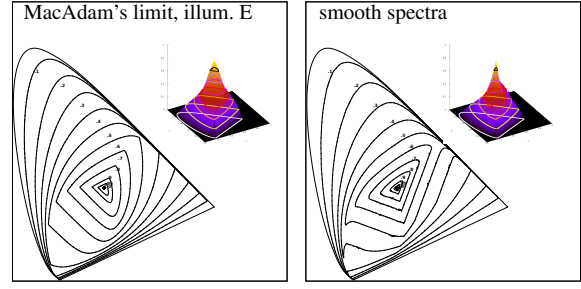


**Figure 5:** Visualisation of the solid of valid (left) and natural (right) reflectances, as a 3D contour plot of brightness  $b = X + Y + Z$  over the base of the  $(x, y)$  chromaticity diagram. MacAdam's limit defines the largest theoretically possible solid, ours corresponds to smooth spectra similar to those occurring with natural materials.

**Implementing MacAdam's Spectra** For comparison, we also implemented an XYZ upsampling algorithm based on the theoretical spectra derived by MacAdam [Mac35a]. In a pre-pass, we store a  $1024 \times 1024$  texture as look-up table, where every pixel represents one  $(x, y)$  chromaticity pair. In a simple nested loop, we enumerate all  $(\lambda_1, \lambda_2)$  pairs which define all possible box functions:  $\lambda_1 \in \Lambda$  is the location of the raising edge,  $\lambda_2 \in \Lambda_2 = (\lambda_1, 730 + (730 - 380)]$  the falling one, defined on the extended domain  $\Lambda_2$  to simplify wrapping around the interval of definition.

For each such pair, we use precomputed cumulative distribution functions of the colour matching functions to quickly compute the integrals to obtain  $(X, Y, Z)$ . From that we derive the chromaticity coordinates of the sample and bin the output data (brightness  $X + Y + Z, \lambda_1, \lambda_2$ ) into the three colour channels of the texture.

During run-time, we do a simple look-up based on the desired chromaticity and reconstruct the spectrum by testing each wavelength  $\lambda$  against the box in the extended domain:  $s(\lambda) = 1$ , if  $\lambda_1 < \lambda \leq \lambda_2$  or  $\lambda_1 < \lambda + (730 - 380) \leq \lambda_2$ , otherwise  $s(\lambda) = 0$ .

#### 4. Solid of Natural Reflectances

Now that we have methods at hand to create smooth spectra by upsampling arbitrary tristimulus color spaces, we can use these methods to define the *solid of natural reflectances*, and introduce mapping techniques to map arbitrary input to this solid (solid mapping), thus ensuring energy conservation.

Following MacAdam [Mac35a], we can define the *solid of valid reflectances* using any method to upsample XYZ to spectra: For every chromaticity  $(x, y)$  we compute a spectrum, and rescale it by a brightness  $b(x, y)$  such that  $b \cdot s(x, y, \lambda) \leq 1 \forall \lambda$ . This value  $b(x, y)$  is the maximum brightness that a colour of this chromaticity can achieve to obey

energy conservation, assuming this underlying model for spectral distributions.

Using MacAdam’s approach and inserting the theoretical optimum (box spectra) results in the largest possible solid, but this will not be a tight bound around the colours of smooth spectra of real materials, and thus look unnatural (see Fig. 3). If we instead make use of our spectra optimised for smoothness, we obtain a smaller solid which we refer to as the solid of natural reflectances. See Fig. 5 for a comparison of the two solid shapes.

We can now use this solid to map a given colour in XYZ to a colour within the solid of natural reflectances (solid mapping).

**Scaling** Scaling the spectrum uniformly such that its maximum is mapped to one preserves smoothness and chromaticity exactly, but may alter brightness drastically. We can use the precomputed map in Fig. 6 as a scaling factor directly:

$$S(s(x, y, \lambda)) = s(x, y, \lambda) \cdot b(x, y), \text{ or} \quad (5)$$

$$S(X, Y, Z) = (X, Y, Z) \cdot b(x, y). \quad (6)$$

Note that using the precomputed  $b(x, y)$  allows to apply scaling directly to the XYZ data without explicitly computing the corresponding spectrum.

**Clipping** Clipping the spectrum at a value of 1 yields a valid reflectance spectrum, however, potentially introducing kinks into the spectrum:

$$C(s(x, y, \lambda)) = \min\{1, s(x, y, \lambda)\}. \quad (7)$$

This is particularly useful for renderers which implement transport based on a single wavelength, continuously chosen by Monte Carlo, because it can be performed for each  $\lambda$  individually.

**Minimal Distortion** This method is more involved than the other two and useful as a reference. It achieves minimum colour shift (in terms of CIE 1976  $\Delta E$  error) by changing both brightness and chromaticity.

$$M(s(x, y, \lambda)) = s(x', y', \lambda), \text{ with} \quad (8)$$

$$(x', y') = \operatorname{argmin} \left\| (X', Y', Z') - (X, Y, Z) \right\|_{\Delta E} \quad (9)$$

Since CIE 1976  $\Delta E$  is the Cartesian distance in the Lab colour space [CIE08], we are geometrically searching for the shortest distance by finding an orthogonal line from the surface of the 3D solid of valid reflectances to the original point  $(X, Y, Z)$  (in Lab space).

We do this using a predictor/corrector method: The predictor projects the current Lab point onto the surface of the solid by converting it to XYZ, applying scaling by  $b(x, y)$  and converting back to Lab. The corrector estimates the normal of the solid surface in Lab space via finite differences and predicts a new point where the distance between the input

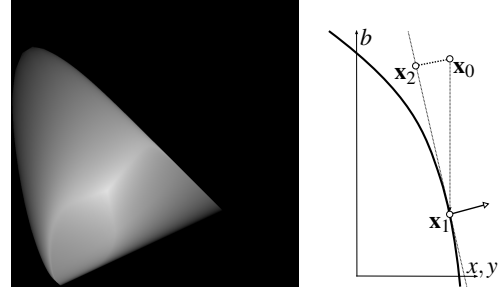


**Figure 6:** Left: precomputed  $b(x, y)$  map storing maximum brightness for each chromaticity. This is used by the predictor/corrector method for  $\min \Delta E$  solid mapping (right): we start at point  $\mathbf{x}_0$  and, in the corrector step, project to the solid boundary at  $\mathbf{x}_1$  by simple scaling by  $b(x, y)$ . Then, a surface normal is estimated and the next step is predicted by computing the point  $\mathbf{x}_2$  with shortest distance to the first-order approximation of the solid surface (in Lab space), and the process repeats.

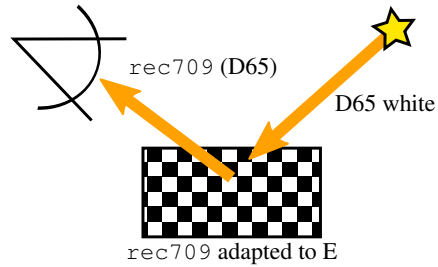


**Figure 7:** Interpretation of a linear sRGB texture. Since it makes little sense to encode a D65 white point for a reflectance (only for the light between the texture and the observer), we reinterpret this input to look the same when observed under D65 illumination.

point and the plane defined by this normal is the smallest (see Fig. 6). The process repeats and usually converges after 3-10 iterations.

Note that only clipping needs to go through spectral representation explicitly, if tristimulus values are to be transformed. All three strategies can be performed for MacAdam’s limit as well as for smooth spectra, by using the corresponding dense map  $b(x, y)$  (Fig. 5 and 6, left). Smits’ method already includes implicit energy conservation and the respective dense map would be almost constant.

## 5. A Colour-Managed Pipeline

**Input** Often input textures are given as sRGB, or linear Rec709, i.e. relative to a D65 white point. Baking a white point into a reflectance is meaningless, since it is a property of the illuminant. Instead, we split up the informa-

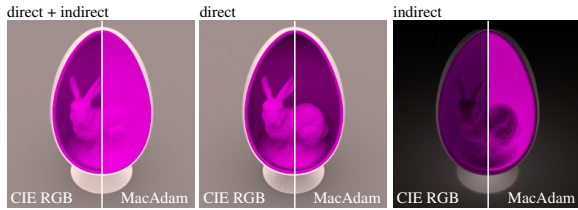


**Figure 8:** Renderings of an object with MacAdam spectrum and corresponding CIE RGB reflectance of (0.44, 0.016, 0.51). While the direct illumination matches, the indirect illumination behaves quite differently for spectral and RGB rendering. For each surface interaction the values of the CIE-*RGB* tristimulus become smaller whereas the spectral values remain 1 for wavelengths  $\in [455, 620]$ .

tion about colour and illuminant by reinterpreting the input colour as the same colour space (Rec. 709 in this example) but adapted to illuminant E. White balancing by scaling (i.e. not using any more sophisticated techniques like Bradford adaptation [Lam85]) works best here, since it does not change the shape of the solid in the  $(x, y)$  chromaticity diagram. This is also the way Smits [Smi99] defined his input colour matrix. It is important to note that the input data stays untouched, only the colour matrix when converting it to XYZ changes.

With this setup, an input colour given as Rec. 709 (1, 1, 1) will result in an equal energy reflectance spectrum, and look like the input texture did on screen while painting it, when illuminated with a D65 light source (see Fig. 7).

**Input Solid Mapping** This input texture data then may need to be mapped into the solid of natural reflectances. Any method will work, but yield slightly different results. In particular, one has to decide whether colour differences or absolute values of correct input are more important to a specific application (see Fig. 11). Note that for parameters of volume transport, this solid mapping needs special attention, since scattering cross sections and mean free paths do not directly describe colours. See Sec. 6 for a discussion.

**Spectral Rendering** When simulating light transport per wavelength, the tristimulus input needs to be upsampled to spectral representation during runtime. When using our grid-based method, we need to re-clip to  $s(x, y, \lambda) \leq 1$  due to the approximate nature of the interpolation between grid points and because the solid shape is not convex. We still recommend mapping the input up front with scaling or using the  $\min \Delta E$  method, to avoid grid artefacts.

**Tristimulus Rendering** When not using spectral transport, it is most physically meaningful to perform transport in colour spaces such as CIE RGB or wide-gamut RGB, since the primaries are mono-wavelength spectral intensities (at 435.8, 546.1, 700nm and 450, 525, 700nm, respectively). This corresponds to simulating three times single-

wavelength spectral transport. Unfortunately this produces results which are very different from simulating the full spectrum, as will any other RGB working space [MMC15] (see Fig. 8 and Fig. 1 in our supplemental material). This is an inherent limitation of tristimulus transport, but we can now provide values which correspond to natural reflectances.

**Output** Converting to the output colour space is straight forward, using the dot product with the colour matching functions for spectral data, or the colour matrix to convert RGB to XYZ. This can be stored in the framebuffer without clamping for further processing and handed over to display colour management.

## 6. Results

All images in our figures are encoded in sRGB for display on commodity monitors, even though the issues with tristimulus reflectances arise especially for colour spaces with wider gamut. We recommend viewing them on screen, some detail may be lost in print.

method	MacAdam	Smits	grid (ours)
time for 10k runs	1700 ms	3342 ms	3314 ms

**Table 1:** Speed comparison of the upsampling methods, fastest of three runs on a Intel i7-2630QM CPU @ 2.00GHz.

**Upsampling Speed** We implemented all three XYZ to spectrum upsampling methods (MacAdam [Mac35a], Smits [Smi99] and the grid-based approach described in Sec. 3) in C. A performance comparison can be seen in Tab. 1. There is no noticeable speed impact of the grid-based approach as compared to Smits’ method. Our implementation of MacAdam’s spectra is very fast, but suffers from quantisation artifacts (see Fig. 9).

**Upsampling Precision** Fig. 9 analyses the precision of the three upsampling techniques, converting XYZ to spectral power distribution and back. The grid uses only a moderately fine  $6 \times 4$ -cell quantisation between white and red here, but the linear interpolation stage still matches the colours exactly (see Eq. (3)).

Smits’ method is not designed to work outside the Rec. 709 gamut, and trades round-trip precision for validity of reflectances even within this gamut. This practical algorithm combines the two goals, optimisation to match colour and energy conservation, in only one step, meeting both goals only partly in the end.

The MacAdam-processed image in Fig. 9 is computed by dividing out the brightness  $b(x, y)$  which we store in the pre-computed map, to undo the baked-in solid mapping by scaling. MacAdam’s construct is of high theoretical interest, but using it in practice is limited by the precision of the colour

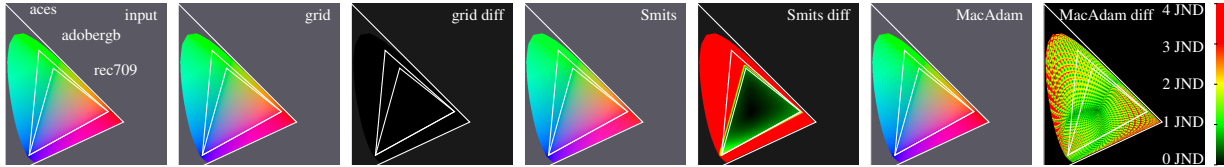


**Figure 9:** A round-trip experiment, upsampling colour to spectral power distribution and converting back. From left to right: input, conversion with the grid-based method and difference image, conversion using Smits’ method and finally MacAdam’s method. The difference is visualised as false colour, indicating perceptual error as multiples of just noticeable differences (JND), where 1 JND is 2.3 CIE 1976  $\Delta E$  (Cartesian distance in Lab space). The gamuts of ACES, AdobeRGB and Rec. 709 are overlaid for better orientation.

matching function tables (even at 1nm bin size). The smallest possible step is to include (or not include) a wavelength bin, incurring substantial steps in  $(x, y)$  chromaticity (hence the quantisation artifacts in Fig. 9). Improving those by linear interpolation would require a tessellation of the  $(\lambda_1, \lambda_2)$  in  $(x, y)$ -space, essentially resulting in the same algorithm as we use for our smooth spectra on a grid, but with more complex topology.

**Mapping to Valid Reflectances** Fig. 10 shows the importance of solid mapping for reflectances. Even at moderate brightness of  $X + Y + Z = 1$  the red corner of the Rec. 709 gamut does not define valid reflectances and needs to be adjusted. This can also be observed in 3D renderings (Fig. 1). Fig. 10 also shows the steep falloff in brightness for colours with  $X + Y + Z = 3$  near the white point  $(1, 1, 1)$ . The more complex method optimising for  $\Delta E$  pays off especially for very saturated tones close to the spectral locus. The grid-based solid mapping methods show some grid interpolation artifacts. We propose that even in a spectral renderer, the input should be solid mapped before upsampling.

**Continuity of the Mapping** Fig. 11 schematically illustrates three mapping strategies (min $\Delta E$ , scaling, and matrix transforms such as [For90]). All three are  $C_1$  continuous, but min $\Delta E$  and scaling introduce kinks in the derivative. Both these map multiple colours outside the solid of valid reflectances to the same output, which might be undesirable. The matrix transform does not introduce these drawbacks, but on the other hand might result in a much smaller output solid and also change perfectly valid input reflectances. For maximum colour accuracy, we think it is best to leave valid reflectances exactly as they were and inform the artist instantly about invalid colours during texture painting.

**Surface Transport** The scene in Fig. 1 consists of four colourful chairs, with diffuse reflectance defined as Rec. 709  $(1, 0.01, 0.1), (1, 0.1, 1), (0.1, 0.1, 1)$  and  $(0.1, 1, 0.1)$ . We show spectral and RGB renders of all combinations of upsampling methods and solid mapping techniques in supplemental material.

**Volumetric Transport** In a render with participating media (Fig. 12), an improvement in tonality can clearly be

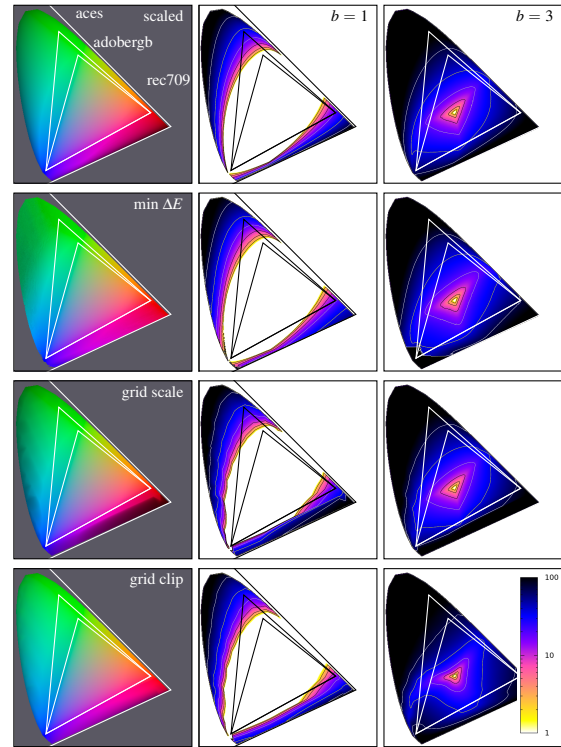


**Figure 10:** Different solid mapping strategies applied to a chromaticity diagram with brightness  $b = 1$  (left two columns) and  $b = 3$ . Even for the limited gamut of Rec. 709, the red primary is outside the solid of valid reflectances, even at moderate brightness. The difference images visualise logarithmic perceptual distance (CIE 1976  $\Delta E$ ) to the unchanged input. The first two rows work directly on the XYZ data, the bottom two first convert the tristimulus values to a spectrum and then perform scaling or clipping.

observed. We rendered the Buddha statue, which is 50cm in height, with a fixed mean free path of 15mm, constant for all wavelengths. It is unclear how to convert mean free paths given as RGB to spectral, since the effect on colour is quite different to a simple multiplication. Thus, we only analyse the effect of defining the scattering albedo  $(\sigma_s/\sigma_t)$  of a homogeneous medium as a colour. The input

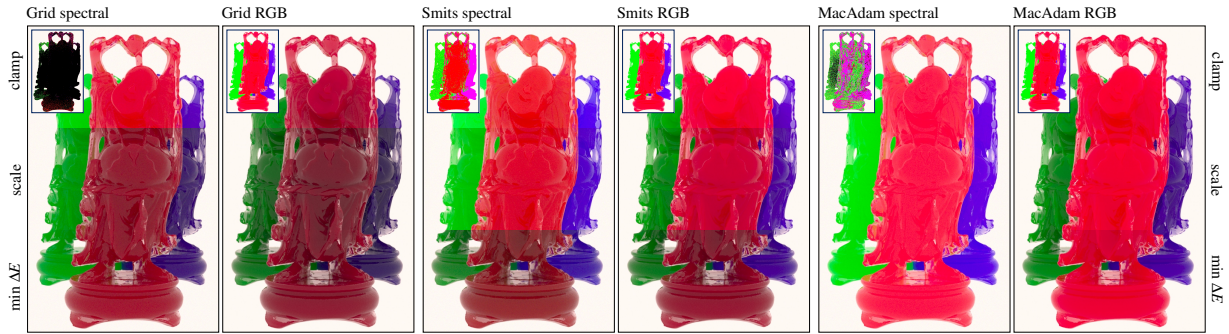


**Figure 12:** Three Buddha statues with coloured scattering and absorbing media. We compare three spectral upsampling methods (each shown in a pair of images) and three methods for ensuring energy conservation (stripes). The uncorrected images are shown as insets. Every other image in the row is obtained using CIE RGB transport, alternating with spectral renders.

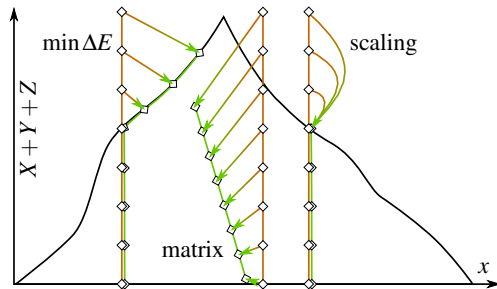


**Figure 11:** Side view of the solid of natural reflectances, with three mapping strategies, illustrating the smoothness of the mapping with respect to albedo. Every line represents input of constant chromaticity coordinate  $(x, y)$  at different albedo and how the mapping affects these colours.

colour space is CIE RGB, and the albedo of the medium is  $(1, 0, 0)$ ,  $(0, 1, 0)$ ,  $(0, 0, 1)$  for the three statues, respectively. Transport is done in CIE RGB or spectral, as indicated.

The small insets represent the four original images without solid mapping, using CIE RGB transport or spectral up-sampled with one of the three methods. Note how the original RGB render looks very flat and shows almost no tonal detail. The grid-upsampled original shows a black image: due to numbers larger than the 32-bit floating point range, the render diverged. Smits’ version shows a strong purple colour cast in the blue statue, and MacAdam’s spectra diverge as well, albeit more slowly.

Spectra generated with Smits’ method are by definition almost energy conserving, and so neither clamping nor scaling have a big effect here. Solid mapping via  $\min \Delta E$  uses again the MacAdam spectra as a basis, and the smooth spectra for the grid-based method.

The greatest effect of solid mapping is visible in spectral transport using the grid method, which is to be expected. Scaling the spectra works best here, both clamping and the  $\min \Delta E$  method exhibit a colour cast. In participating media this is much more severe, since colour saturation accu-

mulates over many more light bounces than in the surface transport case. Note that the RGB version shows almost no detail on the Buddha shape except for what is caused by the Fresnel layer on the interface (this remains true even when stopping down and applying a contrast curve).

## 7. Conclusion and Future Work

We showed that today’s RGB-based rendering pipelines are in general not energy conserving in a physical sense, even though no energy is produced such that the values per RGB channel would increase. That is, the images converge but have no physical counterpart: no real material could produce such colour. We introduced a set of tools and methods to perform solid mapping to the solid of valid reflectances.

Among these tools is a practical XYZ to spectrum up-sampling algorithm which enables fast, per-wavelength access to the spectral power distribution, accepts almost the whole space of visible colours as input, and allows for precise round-trips back to XYZ.

To define the space of natural reflectances, we searched for smooth spectra, assuming no cross-wavelength interactions. Materials can appear brighter and more saturated with fluorescent dyes. While this has been considered in the corresponding literature concerned with printing, light transport becomes significantly more complicated to implement in this case and the effect on colour in indirect light is not easily described in closed form.

The choice of our smoothness term determines the shape of the solid of natural reflectances. While it is motivated by [Smi99], it is arbitrary and there may be a term that produces brighter, yet physically plausible, reflectance spectra.

The grid quantisation of our method comes with slight artifacts when solid mapping has to be performed after up-sampling. If this is an issue for an application, it is simple enough to increase the grid resolution.

Source code for optimisation and upsampling can be found along with the supplemental material.

## References

- [Agl14] AGLAND S.: CG rendering and ACES. <http://nbviewer.ipython.org/gist/sagland/3c791e79353673fd24fa>, 2014. 2
- [BHD\*08] BENDIG M., HANIKA J., DAMMERTZ H., GOLDSCHMIDT J. C., PETERS M., WEBER M.: Simulation of fluorescent concentrators. In *Proc. 2008 IEEE/EG Symposium on Interactive Ray Tracing* (2008), pp. 93–98. 4
- [Cha60] CHANDRASEKAR S.: *Radiative Transfer*. Dover Publications Inc., 1960. ISBN 0-486-60590-6. 1
- [CIE04] *Colorimetry*. Tech. rep., Commission Internationale de l'Éclairage, 2004. 2
- [CIE08] *CIE Colorimetry - part 4: 1976 L\*a\*b\* colour space*. Tech. Rep. ISO 11664-4:2008(E)/CIE S 014-4/E:2007, Joint ISO/CIE Standard, 2008. 6
- [Cou07] COUZIN D.: Optimal fluorescent colors. *Color Research & Application* 32, 2 (2007), 85–91. 4
- [Erm75] ERMAKOW S. M.: *Die Monte Carlo Methode und verwandte Fragen*. VEB Deutscher Verlag der Wissenschaften, 1975. 1
- [FBH98] FAIRMAN H., BRILL M., HEMMENDINGER H.: How the CIE 1931 color-matching functions were derived from wright-guild data. *Color Research and Application* 22, 1 (1998), 11–23. 2
- [FH00] FINLAYSON G. D., HORDLEY S. D.: Improving gamut mapping color constancy. *IEEE Transactions on Image Processing* 9, 10 (2000), 1774–1783. 2
- [For90] FORSYTH D. A.: A novel algorithm for color constancy. *Int. J. Comput. Vision* 5, 1 (Sept. 1990), 5–36. 2, 8
- [Gla94] GLASSNER A.: A model for fluorescence and phosphorescence. In *Proceedings of the 5th Eurographics Workshop on Rendering* (1994), pp. 57–68. 4
- [Gla95] GLASSNER A. S.: *Principles of Digital Image Synthesis*. Morgan Kaufmann, 1995. 3
- [HHA\*10] HULLIN M., HANIKA J., AJDIN B., KAUTZ J., SEIDEL H.-P., LENSCH H.: Acquisition and analysis of bispectral bidirectional reflectance and reradiation distribution functions. *ACM Trans. on Graphics (Proc. SIGGRAPH)* (2010), 1–7. 4
- [Kaj86] KAJIYA J. T.: The rendering equation. *Computer Graphics (Proc. SIGGRAPH)* (1986), 143–150. 3
- [Kra88] KRAFT D.: *A software package for sequential quadratic programming*. Tech. Rep. DFVLR-FB 88-28, Köln, Germany, 1988. 4
- [Lam85] LAM K. M.: *Metamerism and Colour Constancy*. PhD thesis, University of Bradford, 1985. 7
- [Mac35a] MACADAM D. L.: Maximum visual efficiency of colored materials. *Journal of the Optical Society of America* 25, 11 (1935), 361–367. 3, 5, 7
- [Mac35b] MACADAM D. L.: The theory of the maximum visual efficiency of colored materials. *Journal of the Optical Society of America* 25, 8 (1935), 249–249. 3, 4, 5
- [Mal86] MALONEY L. T.: Evaluation of linear models of surface spectral reflectance with small numbers of parameters. *Journal of the Optical Society of America* 3, 10 (1986), 1673–1683. 2
- [Mey88] MEYER G. W.: Wavelength selection for synthetic image generation. *Comput. Vision Graph. Image Process.* 41, 1 (Jan. 1988), 57–79. 3
- [MMC15] MANSENCAL T., MAUDERER M., CANAVAN L.: [http://colour-science.org/blog\\_about\\_rgb\\_colourspace\\_models\\_performance.php](http://colour-science.org/blog_about_rgb_colourspace_models_performance.php), 2015. 7
- [Mor08] MOROVI J.: *Color Gamut Mapping*. Wiley Publishing, 2008. 2
- [Pee93] PEERCY M. S.: Linear color representations for full speed spectral rendering. In *Proceedings of the 20th Annual Conference on Computer Graphics and Interactive Techniques* (New York, NY, USA, 1993), SIGGRAPH '93, ACM, pp. 191–198. 3
- [PH10] PHARR M., HUMPHREYS G.: *Physically Based Rendering: From Theory to Implementation*, 2nd ed. Morgan Kaufmann Publishers Inc., 2010. 1
- [Rec02] *Recommendation ITU-R BT.709-5: Parameter values for the HDTV standards for production and international programme exchange*. Tech. rep., International Telecommunication Union, 2002. 1, 2
- [Sch19] SCHRÖDINGER E.: Theorie der Pigmente größter Leuchtkraft. *Annalen der Physik* 367, 15 (1919), 603–622. 2, 3
- [SFCD99] SUN Y., FRACCHIA F. D., CALVERT T. W., DREW M. S.: Deriving Spectra from Colors and Rendering Light Interference. *IEEE Comput. Graph. Appl.* 19, 4 (July 1999), 61–67. 3
- [SG31] SMITH T., GUILD J.: The C.I.E. colorimetric standards and their use. *Transactions of the Optical Society* 33, 3 (1931), 73–134. 2
- [Smi99] SMITS B.: An RGB-to-spectrum conversion for reflectances. *Journal of Graphics Tools* 4, 4 (1999), 11–22. 3, 7, 9
- [SN07] SUSILA P., NAUS J.: A Monte Carlo study of the chlorophyll fluorescence emission and its effects on the leaf spectral reflectance and transmittance under various conditions. *Photochemical & Photobiological Sciences* 6 (2007), 894–902. 4
- [Sob94] SOBOL' I.: *A Primer for the Monte Carlo Method*. CRC Press, 1994. 1
- [VG95] VEACH E., GUIBAS L. J.: Optimally combining sampling techniques for Monte Carlo rendering. *Proc. SIGGRAPH* (1995), 419–428. 3
- [WEV02] WARD G., EYDELBERG-VILESHIN E.: Picture Perfect RGB Rendering Using Spectral Prefiltering and Sharp Color Primaries. In *Eurographics Workshop on Rendering* (2002), The Eurographics Association. 3
- [WGRK\*97] WELCH A., GARDNER C., RICHARDS-KORTUM R., CHAN E., CRISWELL G., PFEFER J., WARREN S.: Propagation of fluorescent light. *Lasers in Surgery and Medicine* 21 (1997), 166–178. 4
- [WND\*14] WILKIE A., NAWAZ S., DROSKE M., WEIDLICH A., HANIKA J.: Hero wavelength spectral sampling. *Computer Graphics Forum (Proc. Eurographics Symposium on Rendering)* 33, 4 (July 2014), 123–131. 3
- [Wri28] WRIGHT W. D.: A re-determination of the trichromatic coefficients of the spectral colours. *Transactions of the Optical Society* 30, 4 (1928), 141–164. 2
- [WS82] WYSZECKI G., STILES W.: *Color science: concepts and methods, quantitative data and formulae*. Wiley classics library. Wiley, 1982. 1, 2
- [WWLP06] WILKIE A., WEIDLICH A., LARBOULETTE C., PURGATHOFER W.: A reflectance model for diffuse fluorescent surfaces. In *Proceedings of the 4th International Conference on Computer Graphics and Interactive Techniques in Australasia and the Southeast Asia* (2006). 4
- [WXS04] WANG Q., XU H., SUN Y.: Practical construction of reflectances for spectral rendering. In *In Proceedings of the 22th International Conference in Central Europe on Computer Graphics, Visualization and Computer Vision* (2004), pp. 193–196. 4